Journal of Theoretical and Applied Physics (2018) 12:209–217
https://doi.org/10.1007/s40094-018-0297-9

RESEARCH

Peculiar magnetic properties of NC_6 and NC_{12} layered compounds from first principles

Samir F. Matar[1]

Received: 12 April 2018 / Accepted: 19 July 2018 / Published online: 9 August 2018

Abstract
In the context of characterizing nitrogen-poor carbonitrides for different applications, identification of an unusual onset of spin polarization of N(*p*) states has been shown. A full saturation up to 3 μ_B is demonstrated in extended two-dimensional carbon networks of NC_6 and NC_{12} hexagonal structures refined based on density functional theory calculations. From establishing the energy–volume equations of states in both compounds assuming spin-degenerate (non-spin-polarized) and spin-polarized configurations, the ground state is identified as ferromagnetic. The variation of magnetization with volume points to strongly ferromagnetic behavior.

Keywords *p*-Magnetism · DFT · ELF · 2D carbon structure

Introduction

The onset of magnetic polarization requires a significant localization of the states likely to carry a finite magnetic moment. Such localization is illustrated by a high density of states (DOS) at the Fermi level $n(E_F)$ in an initially spin-degenerate electron system configuration. $n(E_F)$ can be quantified from calculations within density functional theory (DFT) [1, 2] and inferred from the Stoner theory of band (ferro)magnetism [3], whereby localization leading to a large $n(E_F)$ magnitude is an indication of unstable electronic system in spin-degenerate configuration (also labeled non-spin-polarized NSP) and it should be stabilized by spin polarization (SP) via dispatching the electrons into two spin populations: majority spins ↑ and minority spins ↓. The difference between ↑ and ↓ spin populations gives a finite magnetic moment. In general, magnetization develops on *d* states of transition metals or *f* states of rare earths and actinides: *nf* (*n* = 4, 5, respectively). Regarding transition metals *nd* (*n* = 3, 4, 5), the first period developing finite magnetization is ferromagnetic metals Fe, Co and Ni, but not metals of second and third periods because their 4*d* and 5*d* bands are too broad to allow for *d* states to localize enough. Also rare earth gadolinium is a ferromagnet at room temperature with $M = 7\ \mu_B$ magnetic moment. Note that while in 3*d* ferromagnetic metals, the onset of the magnetic moment is of interband nature (mediated by the electron gas), in Gd, the moment arises from 4*f* intraband spin polarization.

On the other side, the elements devoid of *d* states have *p* valence external subshells characterized by large spatial expansion, which leaves them little chance for the development of magnetic moment. However, ordered magnetic moments were identified in hexaborides AEB_6 (AE = Ca, Sr) [4] as well as in CdS doped with main group elements [5]. Also, the onset of finite magnetization carried by N-*p* states, thanks to the localization of N(p_z), was recently shown, based on computations within DFT in a layered carbon graphitic-like AlB_2-type NC_2 structure with 1.1 μ_B aligned along *c*-hexagonal axis [6]. The AlB_2-type NC_2 structure (cf. Fig. 1) can also be viewed as a honeycomb arrangement of C sublattice interlayered by N, a feature close to the lithium intercalation compounds [7] used as electrodes in electrochemical processes of battery charge–discharge. In this context, two graphitic anode compositions were identified: LiC_{12} and LiC_6 [8] and characterized by in situ neutron diffraction with layered-like structure within *P6/mmm* space group (like AlB_2-type NC_2), cf. Fig. 1c, d.

Samir F. Matar was formerly at CNRS, University of Bordeaux, ICMCB. 33600 Pessac. France.

✉ Samir F. Matar
s.matar@lgu.edu.lb; abouliess@gmail.com

[1] Lebanese German University (LGU), Sahel-Alma Campus, Jounieh, Lebanon

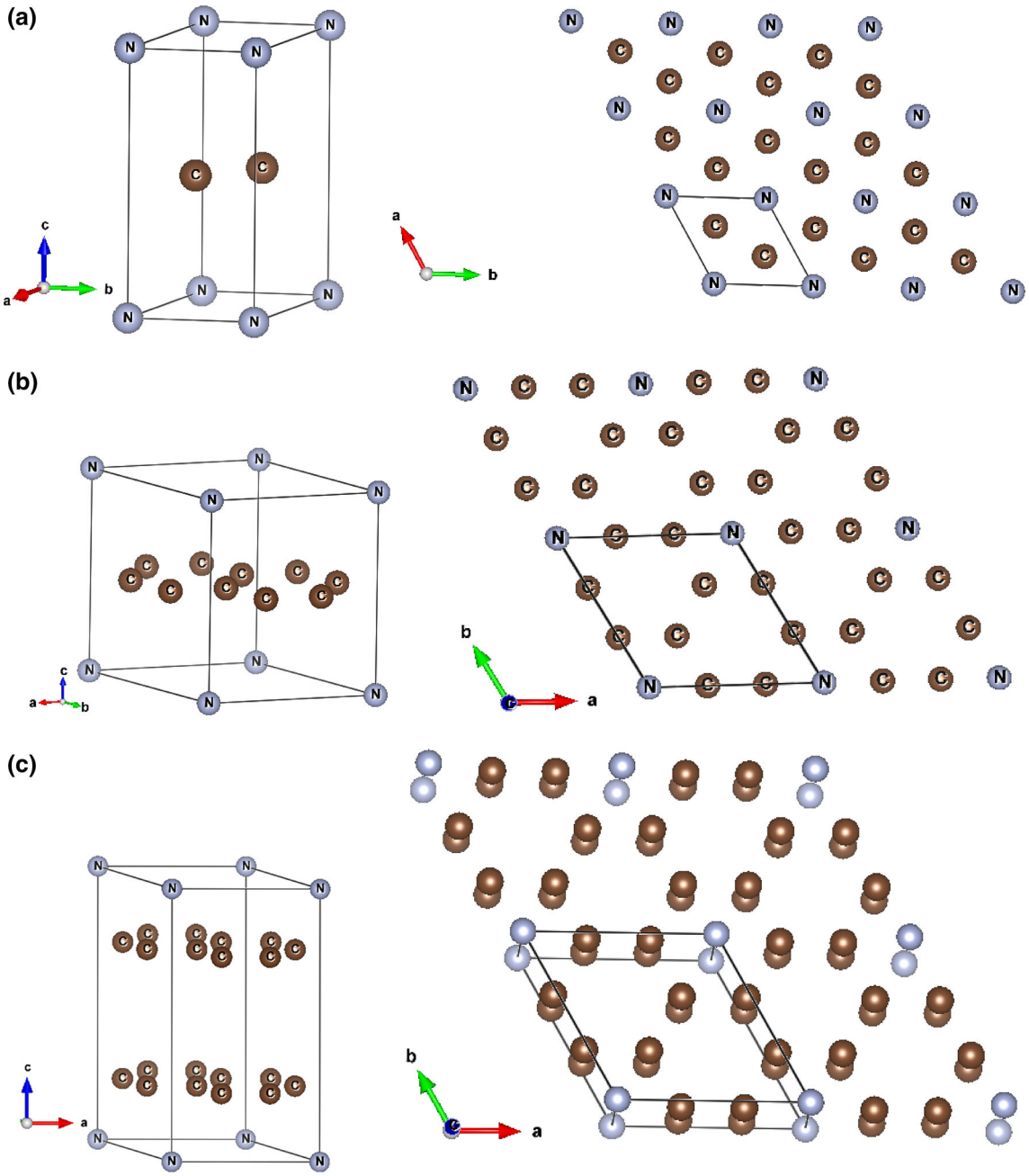

Fig. 1 C_xN layered structures in *P6/mmm* space group shown in simple cell and multiple cell projections to highlight the extended basal plane projection: **a** NC_2 [2], **b** geometry-optimized NC_6 and **c** NC_{12} based on LiC_6 and LiC_{12} experimental structures [3]

Following the unusual results of magnetization of main group elements in certain structural and electronic conditions [4, 5] and of N(*p*) in layered AlB_2-type NC_2 *P6/mmm* [6] on the one hand and the context of extended two-dimensional (2D) carbon network in LiC_6 and LiC_{12} [8] in the same space group as AlB_2–NC_2 (cf. Table 1), it became necessary to further investigate the magnetic behavior of N in such extended 2D carbon networks of NC_6 and NC_{12} (Fig. 1) obtained from geometry optimizations starting from the corresponding Li-based experimental structures.

Also, this study of NC_6 and NC_{12} is inscribed to a certain extent in the context of early investigations more than 25 years ago of nitrogen-poor carbonitrides with CVD/PVD growth experiments aiming at preparing firstly layered and then ultra-hard compounds as $C_{11}N_4$ for applications as coating materials in tooling machinery [9, 10].

The paper reports on such original investigations and shows that the effect of carbon lattice expansion leads to the full polarization of all three N(*p*) electrons with 3 μ_B

Table 1 Layered NC_x (x = 2, 6, 12)

Calculated [6] NSP (SP) NC_2 (AlB_2-type)	Experimental [8] LiC_6	Calculated NSP (SP) NC_6	Experimental [8] LiC_{12}	Calculated NSP (SP) NC_{12}
N(1*a*) 0, 0, 0	Li(1*a*) 0, 0, 0	N(1*a*) 0, 0, 0	Li(1*a*) 0, 0, 0	N(1*a*) 0, 0, 0
a = 2.41 (2.41)	a = 3.68	a = 4.27 (4.26)	a = 4.268	a = 4.265 (4.265)
c = 4.85 (5.32)	c = 4.30	c = 4.42 (5.24)	c = 7. 022	c = 8.078 (8.781)
C(2*d*) 1/3, 2/3, ½	C(6*k*) 0.333, 0, ½	C(6*k*) 0.334, 0, ½	C(12*n*) 0.333, 0, ¼	C(12*n*) 0.336, 0, ¼
d(N–C) = 3.0	d(Li–C) = 2.33	d(N–C) = 2.90 (2.95)	d(Li–C) = 2.26	d(N–C) = 2.46 (2.62)
d(C–C) = 1.39	d(C–C) = 1.44	d(C–C) = 1.42 (1.41)	d(C–C) = 1.43	d(C–C) = 1.42 (1.40)

Space group *P6/mmm*; No. 191. Distances are in units of Å (1 Å = 10^{-10} m)

saturated magnetic moment in a ferromagnetic ground state from energy–volume equations of states and to different magnetovolume behaviors with weak and strong ferromagnetic behaviors of NC_6 and NC_{12}, respectively.

Computation framework

Within DFT plane waves, VASP code [11, 12] was used to geometry optimize atomic positions and lattice parameters leading to ground-state configuration with minimized inter-atomic forces. We performed two sets of calculations considering spin-degenerate (non-spin-polarized NSP) and spin-polarized (SP) configurations for each one of the two carbonitrides NC_6 and NC_{12}. The calculations are based on the projector augmented wave (PAW) method [12, 13] with potentials built within the generalized gradient approximation (GGA) for an account of the effects of exchange and correlation [14]. Within our computational scheme, the conjugate-gradient algorithm [15] was used to relax the atom positions of the different chemical systems into their ground-state structure. The structural parameters were considered to be fully relaxed when forces on the atoms were less than 0.02 eV/Å and all stress components were below 0.003 eV/Å^3. The tetrahedron method with Blöchl corrections [16] was applied for both geometry relaxation and total energy calculations. Brillouin-zone (BZ) integrals were approximated using the special k-point sampling of Monkhorst and Pack [17]. The calculations were converged at an energy cutoff of 500 eV for both compounds. The k-point integration is carried out with a starting mesh of 6 × 6 × 6 up to 10 × 10 × 10 for best convergence and relaxation to zero strains.

Properties relevant to electron localization are obtained from real-space analysis of electron localization function (ELF) according to Becke and Edgecomb [18] which was initially formulated for Hartree–Fock approach and then adapted to DFT methods. ELF is based on the kinetic energy in which the Pauli exclusion principle is accounted for: ELF = $(1 + \chi_\sigma^2)^{-1}$ with $0 \leq \text{ELF} \leq 1$, meaning that ELF is a normalized function. In this expression, the ratio $\chi_\sigma = D_\sigma/D_\sigma^0$, where $D_\sigma = \tau_\sigma - \frac{1}{4}(\nabla\rho_\sigma)^2/\rho_\sigma$ and $D_\sigma^0 = 3/5\,(6\pi^2)^{2/3}\rho_\sigma^{5/3}$ correspond, respectively, to a measure of Pauli repulsion (D_σ) of the actual system and to the free electron gas repulsion (D_σ^0) and τ_σ is the kinetic energy density. In this paper, we use ELF planes along selected orientations of the cell to show differentiated electron localizations with color maps: blue areas for no localization, red for full localization and green for free electron-like localization.

Geometry optimization and energy-dependent results

Geometry optimizations pertain to atomic relaxations with no structural constrains. Starting from the lithium–carbon compounds, iterative calculations led to minimize the inter-atomic forces while keeping the symmetry in *P6/mmm* space group. The protocol was carried out for both spin-degenerate (NSP) and spin-polarized (SP) configurations for each composition.

Electron localization function maps

An illustration of the results after full geometry relaxation is obtained from the electron localization ELF mapping. Figure 2a, b shows the basal plane ELF projection of N contours in NC_6 (top) and NC_{12} (bottom) for four adjacent cells. The color scale shown at the bottom of the figures is from 0 (blue) to 1 (red). The presence of large blue areas between the strong concentrations of electrons around N indicates localization and isolation of individual N. Vertical ELF contour plot at Fig. 2c, d shows the electron concentration around C–C pairs with one layer in NC_6 and two layers in NC_{12} on the one hand and the localization around N along the hexagonal c-axis. Non-vanishing green free electron-like areas indicate bonding between N and C. Lastly, Fig. 2e, f shows for NC_6 and NC_{12} the strong

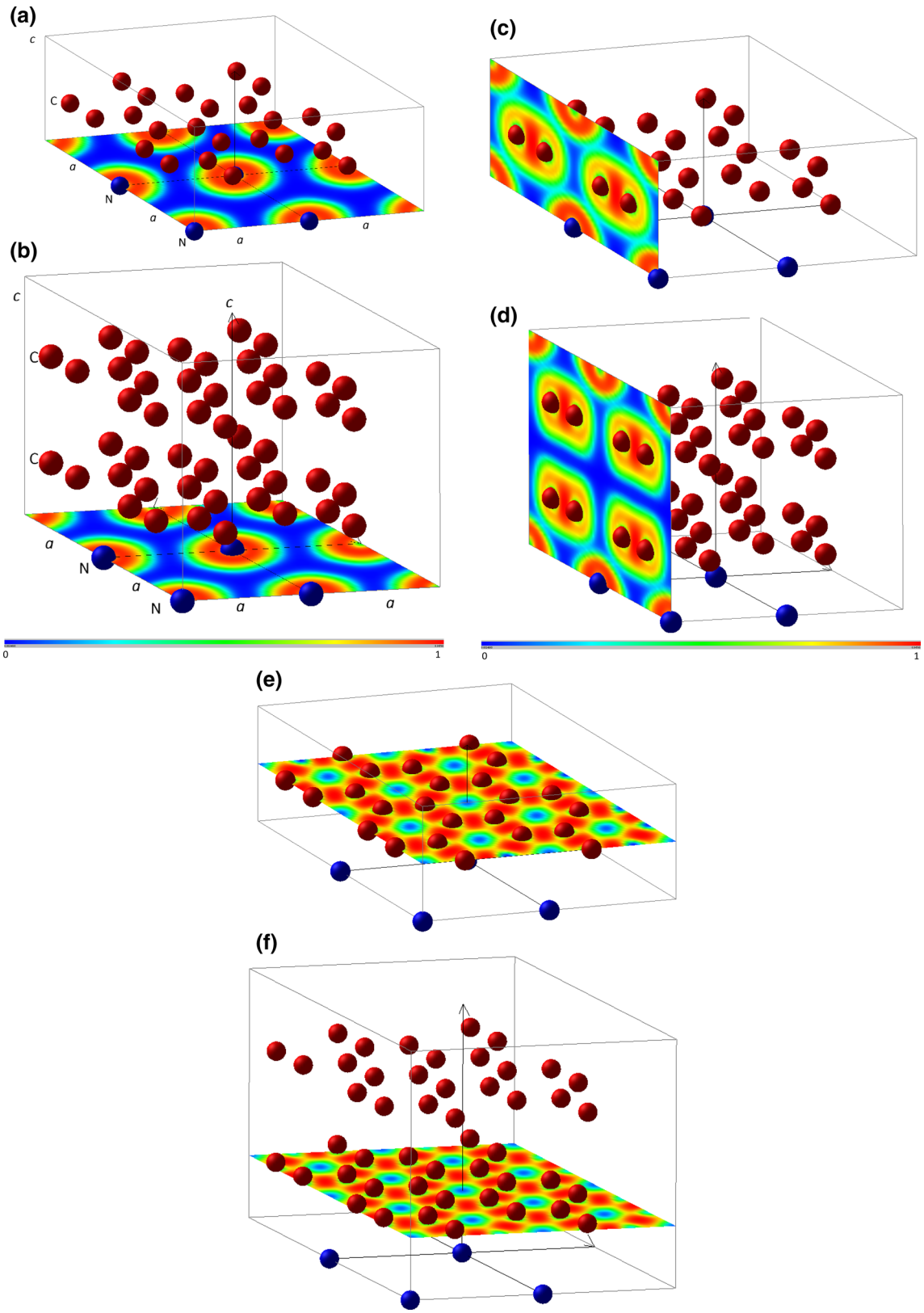

Fig. 2 Electron localization function ELF slices of title compounds: **a**, **c**, **e** for NC_6 and **b**, **d**, **f** for NC_{12}

localization of electrons between C–C in honeycomb-like carbon network.

Energy-related results analyses

Table 1 provides the starting crystal data of LiC_6 and LiC_{12} used to optimize the corresponding carbonitrides in both spin configurations, NSP and SP. Also for the sake of completeness, the data of NC_2 are included at first column. The x internal coordinate of carbon as well as the C–C distances changes little from Li to N cases meaning that the carbon host network undergoes negligible changes [even for NC_2 with a single C–C pair and where d(C–C) is only slightly smaller]. a lattice parameter changes little from NC_6 to NC_{12} on the one hand and from NSP to SP magnetic configuration on the other hand. This implies that the a parameter defining the horizontal planes is hexagonal lattice, which is controlled by the carbon network.

Using the NSP calculations, trends of cohesive energies E_{coh} were established within the NC_x series averaged as per one atom for better comparison. N and C energies were calculated based on the atom placed in a cubic box. Then, $E(N) = -6.830$ eV and $E(C) = -7.11$ eV. From the energy optimization, $E_{Tot.}(NC_6) = -56.44$ eV and $E_{Tot.}(NC_{12}) = -111.446$ eV, while $E_{Tot.}(NC_2) = -21.52$ eV. Then, the cohesive energies are averaged as per one atomic constituent to enable trends. They amount to (in eV/at.): $E_{coh.}(NC_2) = -0.16$ eV/at.; $E_{coh.}(NC_6) = -0.99$ eV/at.; $E_{coh.}(NC_{12}) = -1.48$/at. The increase in cohesive energy is in line with the extension of the carbon network, and while it is almost 6 times from NC_2 to NC_6, it amounts to 33% from NC_6 to NC_{12} which is most cohesive.

Major changes are observed from NSP to SP for the c-hexagonal parameter. This was equally observed for NC_2 (1st column). The outcome is that the volume of the cell is larger in the spin-polarized configuration as a consequence of the onset of magnetization on nitrogen which amounts to $M = 3\ \mu_B$ in both NC_6 to NC_{12} compounds. Note that in NC_2 $M = 1.1\ \mu_B$.

One first observation that can be proposed is that $M(NC_2) = 1.1\ \mu_B$ is not a saturated magnetization and that saturation requires an extended carbon network such as the one in NC_6 to NC_{12} where it amounts to $3\ \mu_B$, i.e., with the polarization of all three p electrons. Somehow this agrees with the situation of rare earth (RE) Gd where the $7\ \mu_B$ magnetic moment arises from the seven electrons of the 4f-half filled subshell. With this parallel approach, it can be suggested that alike RE p-magnetization here is equally of intraband polarization nature. We shall further develop on this original observation in next sections.

Spin-degenerate density of states (DOS) and origin of the magnetic instability

The origin of the spin polarization should be assessed based on the projection of the spin-degenerate NSP DOS. Figure 3 top panel shows the site-projected DOS for NC_6 exemplarily. The DOS of N and all six carbons are projected. The energy reference along x-axis is with respect to the Fermi level E_F which is crossed by a large N-DOS, whereas C shows little contribution with nevertheless a small peak following the shape of N-DOS whence the quantum mixes between C and N leading to the chemical bonding. As stated in Introduction, such large $n(E_F)$ magnitude which is of p-character (s-states are far lower in energy) is an indication of unstable electronic system in spin-degenerate state. The role of each orbital is shown by the decomposition over p_x, p_y and p_z in the lower panel of Fig. 3. Two kinds of p-DOS can be seen, two degenerate in plane p_x and p_y, broader (notice the DOS shoulder) than out-of-plane p_z which resembles more the carbon DOS at E_F. These results mirror the ELF projections in Fig. 2 where panels (a) and (b) show the p_x and p_y ELF isolated

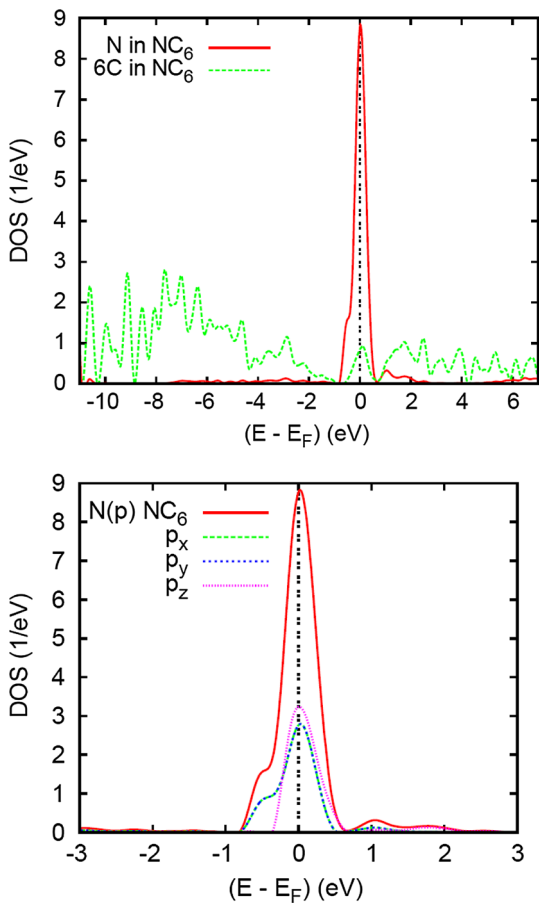

Fig. 3 NSP site-projected DOS in NC_6 and N(p) states projected over x, y and z components

from carbon, whereas panels (c) and (d) exhibit finite ELF between N and C–C pairs while bonding. Then, all three N(p) contribute to the instability which eventually leads to magnetic polarization. As a matter of fact, subsequent SP calculations lead to the onset of magnetization of 3 μ_B in both carbonitrides. The illustration of such integer magnetization identified in both compounds is illustrated in Fig. 4 by the spin-projected (UP ↑ and DOWN ↓) total DOS where the Fermi level is now in a small gap in NC_6 and slightly larger but well defined in NC_{12}, implying that the three p electrons are fully polarized as UP ↑ spins. These are called majority spins because the corresponding DOS are shifted to lower energy versus DOWN ↓ (minority spins) shifted to higher energy as can be seen in the SP DOS plots. Consequently, starting from the high DOS at E_F in the NSP calculations (Fig. 3), the electron system relaxes to a SP ground by reducing the large $n(E_F)$ magnitude. The two compounds are then predicted as ferromagnetic semiconductors. This behavior is close to that observed for C_2O and CrO_2 [19] which are strong half metallic ferromagnets as well as $Co_3Sn_2S_2$ [20, 21].

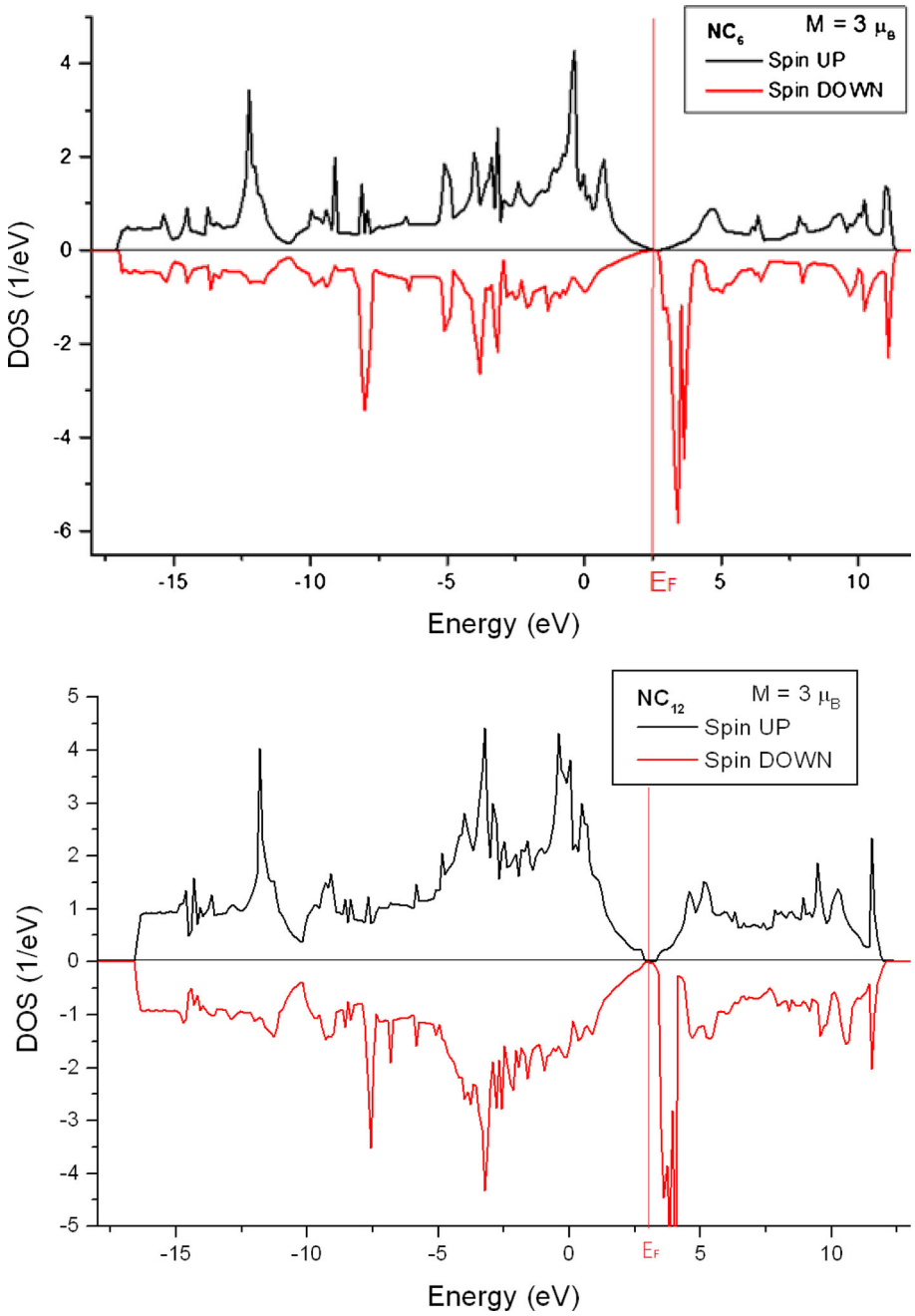

Fig. 4 Spin-projected total DOS of ferromagnetic NC_6 and NC_{12}

Energy–volume equations of state- and volume-dependent magnetic behavior

At this point, the evaluation of the impact of volume changes upon the onset and change of magnetization requires the assessment of the energy–volume equation of states (EOS) of each compound in its two magnetic configurations NSP/SP with calculations around minima found from geometry optimization (Table 1). The resulting curves are plotted in Fig. 5. In both compounds, the ground-state configuration is magnetic (SP) with large stabilization versus NSP: $\Delta E_{NC_6}(SP - NSP) = -1.91$ eV/cell and $\Delta E_{NC_{12}}(SP - NSP) = -2.19$ eV/cell, and the stabilization for NC_{12} is much larger.

The fit of the curves which show a quadratic behavior is done with third-order Birch EOS [22]:

$$E(V) = E_o(V_o) + [9/8]V_oB_o\left[([(V_o)/V])^{2/3}-1\right]^2 + [9/16]B_o(B'-4)V_o\left[([(V_o)/V])^{2/3}-1\right]^3$$

where E_o, V_o, B_o and B'—the fit parameters—are, respectively, the equilibrium energy, the volume, the bulk modulus and its pressure derivative. The obtained corresponding values are given in the insert. χ^2 is the goodness-of-fit indicator.

One first result is the difference of magnitudes between bulk modules, larger for NC_{12} for both NSP and SP on the one hand and the decrease in B_0(SP) versus B_0(NSP) accompanying the reverse trends of volume; i.e., the larger the volume, the smaller the bulk modulus. The SP/NSP crossovers are at 70 and 120 Å^3 volume magnitudes for NC_6 and NC_{12}.

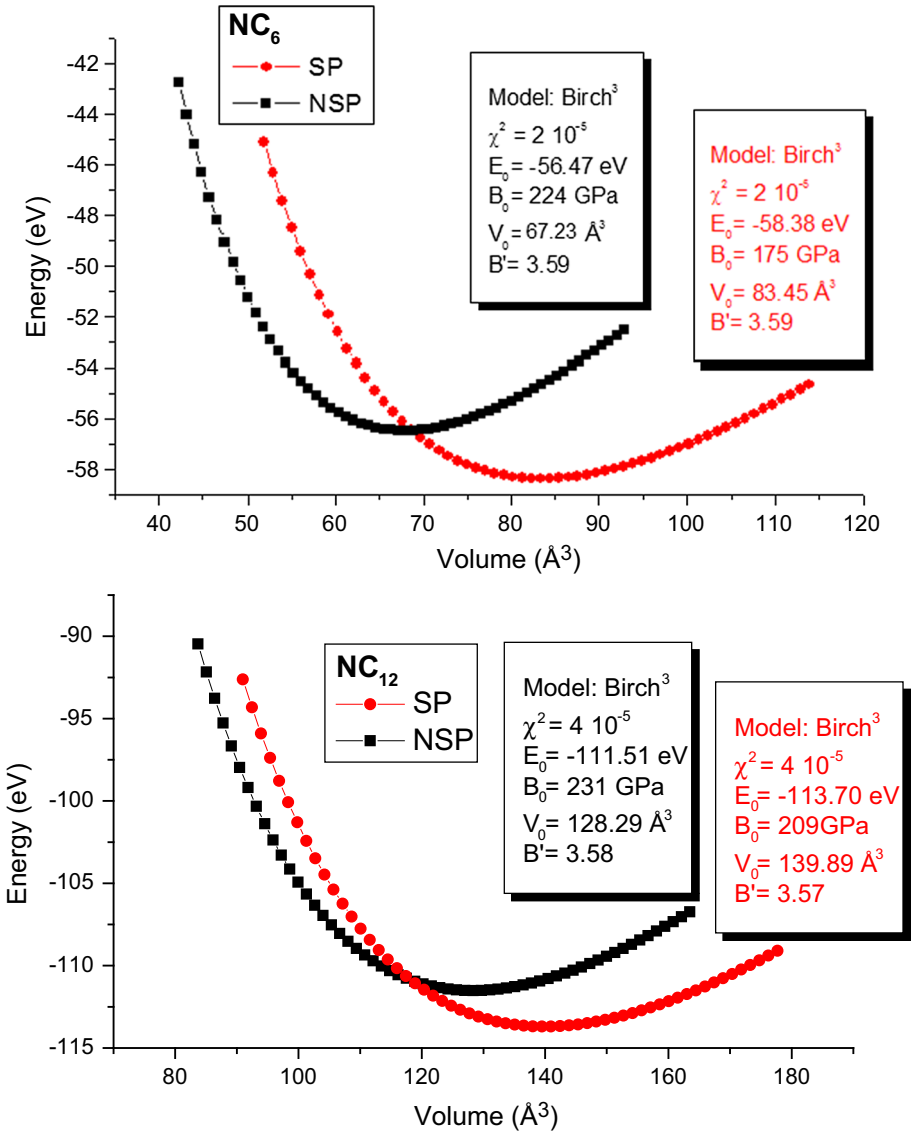

Fig. 5 Energy–volume curves of NC_6 and NC_{12} in non-spin-polarized (NSP) and magnetically ordered (spin-polarized SP) configurations. In both, the ground state is SP (ferromagnetic) at larger volume than NSP

The results can be further assessed by plotting the magnetization as function of volume. The scattered points shown in Fig. 6 present a different behavior at low volume, i.e., with a progressive increase in NC_6 and a much steeper increase in NC_{12} both tending to 3 μ_B, which is in both carbonitrides the saturation magnetization. Note however that saturation is reached in NC_{12} before the NSP/SP crossover line opposite to NC_6 where magnetization collapses right at the vertical red line of crossover. Then it can be suggested that NC_{12} is a stronger ferromagnet than NC_6.

Conclusion

In spite of the focus of present work on the magnetic properties of binary carbon-rich NC_x with results that encourage synthesis endeavor, the topic is yet inscribed to a certain extent in the context of early investigations more than 25 years ago of nitrogen-poor carbonitrides in a European Network for the search of new ultra-hard materials. The know-how-to in synthesizing such compositions with modern CVD/PVD and other growth techniques leading for instance to original compositions as $C_{11}N_4$

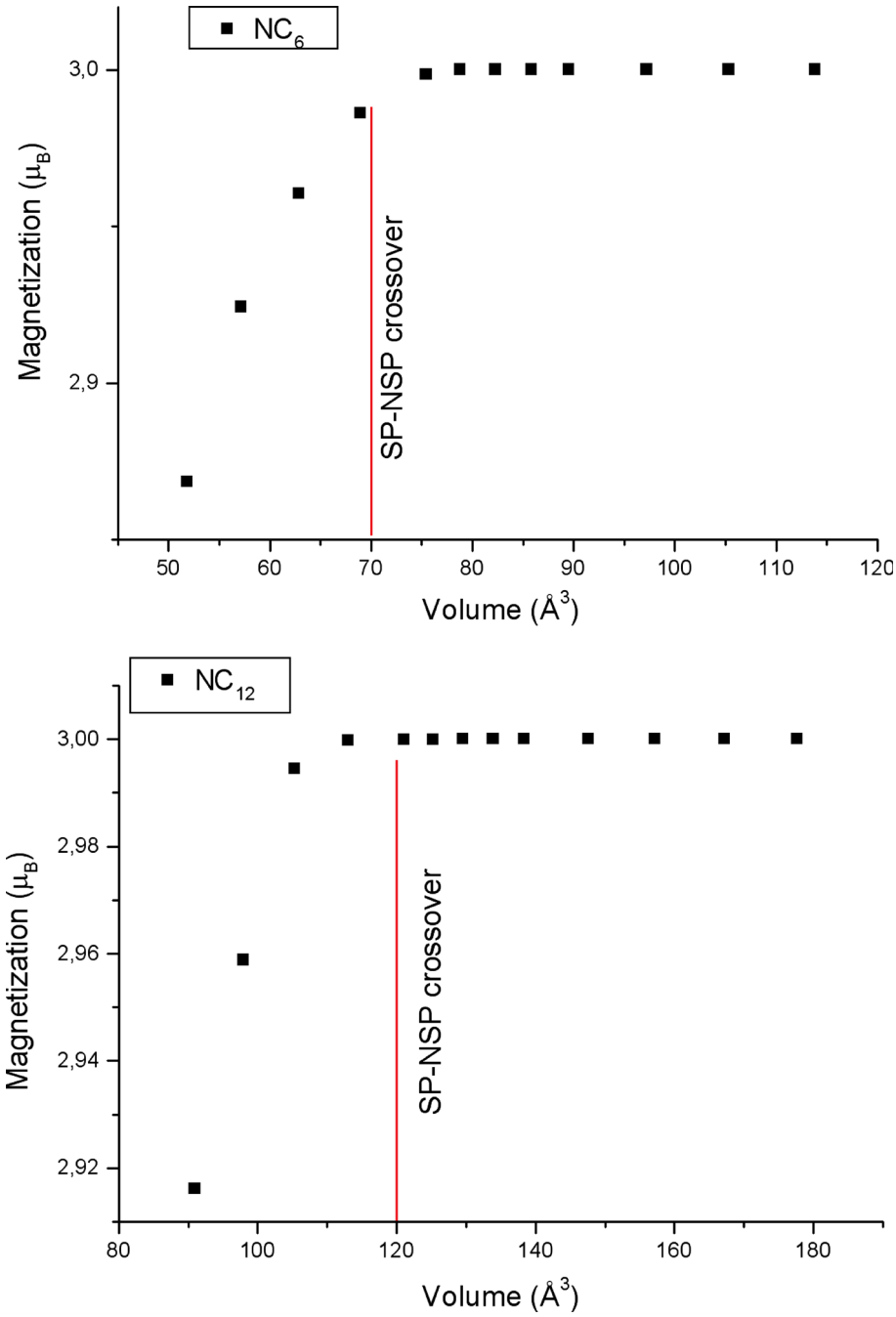

Fig. 6 Variation of the magnetization with cell volume in NC_6 and NC_{12}

carbonitride in both 2D and 3D forms [9, 10] may cast confidence that further growth experiments with smaller amounts of nitrogen might lead to new nitrogen-deficient carbonitrides with compositions ranging from NC_6 to NC_{12} which can be then proposed to the physics community for further characterization, especially the unusual magnetic behavior.

References

1. Hohenberg, P., Kohn, W.: Inhomogeneous electron gas. Phys. Rev. B **136**, 864 (1964)
2. Kohn, W., Sham, L.J.: Self-consistent equations including exchange and correlation effects. Phys. Rev. A **140**, 1133 (1965)
3. Mohn, P.: Magnetism in the Solid State—An Introduction. Springer, Heidelberg (2003). **(Springer Series in Solid-State Sciences)**
4. Dorneles, L.S., Venkatesan, M., Moliner, M., Lunney, J.G., Coey, J.M.D.: Magnetism in thin films of CaB_6 and SrB_6. Appl. Phys. Lett. **85**, 6379 (2004)
5. Bedolla, P.O., Gruber, C., Mohn, P., Redinger, J.: *p*-Electron magnetism in CdS doped with main group elements. J. Phys. Condens. Matter **24**, 476002 (2012)
6. Matar, S.F.: Unusual onset of *p*-element magnetization in a two dimensional structure. Solid State Sci. **60**, 55 (2016)
7. Siegel, R., Hirschinger, J., Carlier, D., Matar, S.F., et al.: ^{59}Co and ^{6,7}Li MAS NMR in polytypes O2 and O3 of $LiCoO_2$. J. Phys. Chem. B **105**, 4166 (2001)
8. Dolotko, O., Senyshyn, A., Mühlbauer, M.J., Nikolowski, K., Ehrenberg, H.: Understanding structural changes in NMC Li-ion cells by in situ neutron diffraction. J. Power Sources **255**, 197 (2014)
9. Mattesini, M., Matar, S.F.: Density-functional theory investigation of hardness, stability, and electron-energy-loss spectra of carbon nitrides with $C_{11}N_4$ stoichiometry. Phys. Rev. B **65**, 075110 (2002)
10. Mattesini, M.: Ph.D. thesis. No. 2429. University of Bordeaux—France (2001)
11. Kresse, G., Furthmüller, J.: Efficient iterative schemes for ab initio total-energy calculations using a plane-wave basis set. Phys. Rev. B **54**, 11169 (1996)
12. Kresse, G., Joubert, J.: From ultrasoft pseudopotentials to the projector augmented-wave method. Phys. Rev. B **59**, 1758 (1999)
13. Blöchl, P.E.: Projector augmented-wave method. Phys. Rev. B. **50**, 17953 (1994)
14. Perdew, J., Burke, K., Ernzerhof, M.: Generalized gradient approximation made simple. Phys. Rev. Lett. **77**, 3865 (1996)
15. Press, W.H., Flannery, B.P., Teukolsky, S.A., Vetterling, W.T.: Numerical Recipes. Cambridge University Press, New York (1986)
16. Blöchl, P.E., Jepsen, O., Anderson, O.K.: Improved tetrahedron method for Brillouin-zone integrations. Phys. Rev. B **49**, 16223 (1994)
17. Monkhorst, H.J., Pack, J.D.: Special points for Brillouin-zone integrations. Phys. Rev. B **13**, 5188 (1976)
18. Becke, A.D., Edgecombe, K.E.: A simple measure of electron localization in atomic and molecular systems. J. Chem. Phys. **92**, 5397 (1990)
19. Matar, S.F., Weihrich, R.: Strong *p*-magnetism in carbon suboxide C2O devised from first principles. Chem. Phys. Lett. **674**, 115 (2017)
20. Weihrich, R., Anusca, I., Anorg, Z.: Half antiperovskites. III. Crystallographic and electronic structure effects in $Sn_{2-x}In_xCo_3S_2$. Allg. Chem. **632**, 1531 (2006)
21. Schnelle, W., Leithe-Jasper, A., Rosner, H., Schappacher, F.M., Pöttgen, R., Pielnhofer, F., Weihrich, R.: Ferromagnetic ordering and half-metallic state of $Sn_2Co_3S_2$ with the Shandite-type structure. Phys. Rev. B **88**, 144404 (2013)
22. Birch, F.: Finite strain isotherm and velocities for single-crystal and polycrystalline NaCl at high pressures and 300 K. J. Geophys. Res. **83**, 1257 (1978)